NRC Research Press

ARTICLE

Eco-friendly recycled crushed glass for cushioning boulder impacts[1]

Y. Su, C.E. Choi, C.W.W. Ng, C. Lam, J.S.H. Kwan, G. Wu, J. Huang, and Z. Zhang

Abstract: A large amount of waste glass is generated every year and contributes significantly to landfills. Large-scale physical model tests were carried out to study the dynamic response of recycled crushed glass (RCG) contained in gabion baskets and its performance against successive boulder impacts at energy levels of up to 70 kJ. The cushioning performance of RCG is compared with that of more conventional cushioning materials, including rock fragments and cellular glass aggregates. Results reveal that for the first impact, RCG can provide up to 144% and 128% reduction in the transmitted wall loads and boulder impact loads, respectively, when compared with cushion layers comprising rock fragments. It follows that by adopting RCG, practitioners could potentially reduce the recommended design load for impact by a single boulder by up to three times. Furthermore, the load-diffusion angle of RCG is three times larger than that of cellular glass aggregates. The observed trend in the diffusion angle implies that the transmitted load for RCG is distributed more uniformly on the barrier wall compared to cellular glass aggregates.

Key words: boulder impact, recycled crushed glass, cushioning material, debris flow, barrier wall.

Résumé : Une grande quantité de déchets de verre est générée chaque année et contribue de manière significative aux décharges. Des essais sur modèle physique à grande échelle ont été réalisés pour étudier la réponse dynamique du verre concassé recyclé (VCR) contenu dans des paniers de gabions et sa performance face aux impacts de blocs successifs à des niveaux d'énergie pouvant atteindre 70 kJ. Les performances d'amortissement du VCR sont comparées à celles de matériaux d'amortissement plus classiques, notamment les fragments de roche et les agrégats de verre cellulaire. Les résultats révèlent que, pour le premier impact, VCR peut réduire de 144 et 128 % les charges transmises aux murs et aux impacts de blocs, respectivement, par rapport aux couches de protection comprenant des fragments de roche. Il s'ensuit qu'en adoptant le VCR, les praticiens pourraient potentiellement réduire jusqu'à trois fois la charge de calcul recommandée pour l'impact par un seul rocher. De plus, l'angle de charge-diffusion du VCR est trois fois plus grand que celui des agrégats de verre cellulaire. La tendance observée dans l'angle de diffusion implique que la charge transmise pour le VCR est répartie plus uniformément sur la paroi de la barrière par rapport aux agrégats de verre cellulaire. [Traduit par la Rédaction]

Mots-clés : impact de rocher, verre concassé recyclé, matériau de rembourrage, coulée de débris, mur barrière.

Introduction

Debris flows occur in multiple surges (Iverson 1997) and large boulders entrained within the flow mass (Takahashi 2014) can severely damage mitigation structures situated along its flow paths (Zhang et al. 1996). To protect these structures, cushion layers can be used to attenuate concentrated forces induced by boulders (Lambert et al. 2009).

Rock fragments contained in gabion baskets, also known as rock-filled gabions (Kwan et al. 2019), are commonly used to protect rockfall mitigation structures (Lambert et al. 2009, 2014). Schellenberg et al. (2007), Heymann et al. (2010), and Breugnot et al. (2015) have demonstrated that rock fragments are very effective at attenuating single boulder impacts. However, the change in bulk stiffness of the cushion layer due to compaction under successive impacts (ASTRA 2008) is often ignored in current design. Ng et al. (2016) demonstrated that the reduction of impact loads rely predominantly on the irreversible rearrangement of rock fragments. The mechanism of crushing in gabion cushioning layers strongly depends on mechanical properties of the rocks and their size (Lambert et al. 2009). Correspondingly, the contact surface between the boulder and the gabion cell contained with rock fragments increases progressively with successive impacts, leading to a reduction in the cushioning performance in terms of the boulder impact force.

Generally, the particle sizes of the rock fragments used to construct gabion cushion layers range from 160 to 300 mm (GEO 1993; Ng et al. 2016). Zhang et al. (2016) and Su et al. (2019) both showed that the transmitted load on a rigid barrier that is shielded by a

Received 3 April 2018. Accepted 14 November 2018.

Y. Su,* J. Huang, and Z. Zhang. JSTI Group, No. 8 East Fuchunjiang Road, Nanjing, China.
C.E. Choi† and C.W.W. Ng.‡ Department of Civil and Environmental Engineering, The Hong Kong University of Science and Technology, Clear Water Bay, Kowloon, Hong Kong.
C. Lam and J.S.H. Kwan. Geotechnical Engineering Office, Civil Engineering and Development Department, Hong Kong SAR Government, Civil Engineering and Development Building, 101 Princess Margaret Road, Kowloon, Hong Kong.
G. Wu. Key Laboratory of Concrete and Prestressed Concrete Structures of the Ministry of Education, Southeast University, Nanjing 210096, China.
Corresponding author: Clarence E. Choi (email: ceclarence@ust.hk).
*Present address: College of Water Conservancy and Hydropower Engineering, Hohai University, 1 Xikang Road, Nanjing 210024, China.
†Present address: Department of Civil Engineering, The University of Hong Kong, Hong Kong.
‡C.W.W. Ng currently serves as an Associate Editor; peer review and editorial decisions regarding this manuscript were handled by E. Alonso.
[1]This paper is part of a Special Issue entitled "Advances in landslide understanding".

Published at www.nrcresearchpress.com/cgj on 23 November 2018.

cushion layer comprising rock fragments (rock-filled gabions) decreases with the particle size, although particle crushing was not considered in these studies. Comparisons between measured and computed results show that when crushing is limited, the mechanical response of a cushioning layer depends on the degree of compaction. This relationship can be used to explain how successive impacts lead to a reduction in cushion efficiency for attenuating the force transmitted to the mitigation structure under protection. Neither Zhang et al. (2016) nor Su et al. (2019) considered the mechanism of crushing in their studies due to the input parameters and simplifications involved. For instance, clear input parameters are required for bonding several spherical particles together (Bertrand et al. 2005) and this emerging research area still presents challenges in discrete element method (DEM) modelling. Based on the results of these previous studies, smaller particle sizes were recommended to improve the overall performance of the cushion layer. With this in mind, there clearly remains potential to explore new granular cushioning materials that can dissipate energy more effectively.

The advent of the development of cushioning materials that are not only sustainable but can also outperform rock-filled gabions has led to the use of waste tires as cushion layers. For example, Lambert et al. (2009) carried out a series of large-scale drop tests, for a single impact, at an energy level of 13.5 kJ on a 0.5 m thick cushioning cell made up of 30% waste tires and 70% sand. The test results revealed that when the boundary condition of the cushioning material was confined, the maximum boulder impact force was up to 30% higher than that of an equivalent rock-filled gabions cushion layer. This implies that sand – waste tire mixtures are not as effective as rock fragments in attenuating boulder impacts.

In recent years, cellular glass aggregates contained in the gabion baskets have also been used as a cushioning material for rockfall protection galleries (Schellenberg et al. 2007; ASTRA 2008). Schellenberg et al. (2006) carried out a series of drop tests on a 0.45 m thick cellular glass aggregates cell at an energy level of 12.5 kJ. The results revealed that cellular glass aggregates can reduce the maximum boulder impact force by up to 40% when compared with that of an equivalent gravel cushion layer. Given the success of cellular glass aggregates in attenuating impact forces, Ng et al. (2018) carried out pendulum impact tests to compare the cushioning performance between gabion baskets filled with cellular glass aggregates and rock fragments. The test results demonstrated that the use of cellular glass aggregates reduced the maximum boulder impact and transmitted forces by up to 25% and 50%, respectively. Despite the promising results for cellular glass aggregates, they exhibited very large plastic deformation beyond their crushing strength and the cushioning efficiency diminished rapidly during successive loading. In addition, manufacturing cellular glass aggregates is an energy-consuming process as it requires baking glass fines with chemical additives.

The demand for glass products is increasing rapidly around the world. Consequently, the amount of waste glass sent to landfills is also increasing. For example, in 2011 glass beverage bottles contributed to about 63% of the waste glass generated in Hong Kong (So et al. 2016). The high generation rate coupled with a low recycling rate means that about 98% waste glass will remain buried in landfills in Hong Kong (Lam et al. 2007). Furthermore, heavy metals such as lead, barium, and strontium contained in waste glass can also pollute the environment and can even pose a threat to human health (Méar et al. 2006; Shi et al. 2005). Given the environmental problem posed by waste glass, recycled crushed glass (RCG) is evaluated as an alternative cushioning material in this study. RCG has been used as coarse aggregates in concrete (Lam et al. 2007; Srivastava 2014) and also as an engineering fill in reclamation and earthworks projects (So et al. 2016). Despite these previous applications, RCG has not been explored as a cushioning material against rockfall or debris flow hazards. The advantage of RCG is that it is easy to manufacture and can be made by simply crushing waste glass using a hammer mill. As will be shown in this study, when subjected to impacts RCG shows both grain rearrangements and crushing, which are the cushioning mechanisms exhibited by rock fragments and cellular glass aggregates as shown in previous investigations. In this study, the cushioning performance of RCG under successive boulder impacts is investigated using a large-scale pendulum impact setup described by Ng et al. (2016) and Lam et al. (2018).

Hertz impact equation

The boulder impact force acting on a rigid reinforced concrete barrier is traditionally estimated using the Hertz contact theory (Johnson 1985), where contact between the boulder and barrier is assumed to be elastic and the contact force is expressed as follows:

$$F = \frac{4E}{3}R^{1/2}(\delta)^{3/5} \tag{1}$$

where F is the impact force (N), E is the effective elastic modulus (Pa), R is the boulder radius (m), and δ is the elastic deformation (m). E is given as $1/E = (1 - \nu_1^2)/E_1 + (1 - \nu_2^2)/E_2$, where E_1 and E_2 are the elastic moduli of barrier and concrete boulder, respectively (in Pa); ν_1 and ν_2 are the Poisson's ratios of barrier and concrete boulder, respectively.

To facilitate the design of rigid debris-resisting barriers in Hong Kong, a simplified Hertz equation was proposed by Kwan (2012)

$$F = K_c\, 4000v^{1.2}R^2 \tag{2}$$

where v is the impact velocity (in m/s) and K_c is an empirical load-reduction factor to take into account the energy dissipation through plastic deformation. Following the advice of Hungr et al. (1984), Kwan (2012) proposed that the value of K_c be taken as 0.1 if the barrier is not protected by a cushion layer. For rigid barriers protected by a rock-filled gabion cushion layer, Ng et al. (2016) carried out physical impact tests and back-calculated the load-reduction factor for successive impacts. The load-reduction factor was found to range from 0.012 to 0.037 at an energy level of 70 kJ. Based on these test results and also the result of a numerical parametric study, Kwan et al. (2019) showed that, for the first boulder impact on a rock-filled gabion layer, the peak boulder impact force could be conservatively estimated using a revised form of the simplified Hertz equation: $F = 100v^{1.2}R^2$.

Large-scale field tests

Impact test setup

Figures 1*a* and 1*b* show front and side views of the test setup, respectively. A 2000 kg reinforced-concrete boulder was connected to a steel frame using two steel strand cables. The steel frame was 6 m in height, 5 m in length, and 3 m in width. A mechanical latch was used to release the boulder from its suspended position into the cushioning material. A steel frame was also erected around the perimeter of the wall to confine the cushion layer. The impact duration for each test was about 0.1 s.

Instrumentation

Eight load cells (THD-50K-Y) with a maximum range of 220 kN were installed on the rigid barrier to measure the load distribution along the horizontal and vertical axes (Fig. 2). An accelerometer (PCB) was used to capture the time history of the acceleration of the concrete boulder (maximum range: 500g, where g is gravitational acceleration). The measured acceleration included the actual physical response between the boulder and cushion layer plus electrical noise. Fast Fourier transform (FFT) signal process-

Fig. 1. Impact test setup: (*a*) front view; (*b*) side view; (*c*) detail view. [Colour online.]

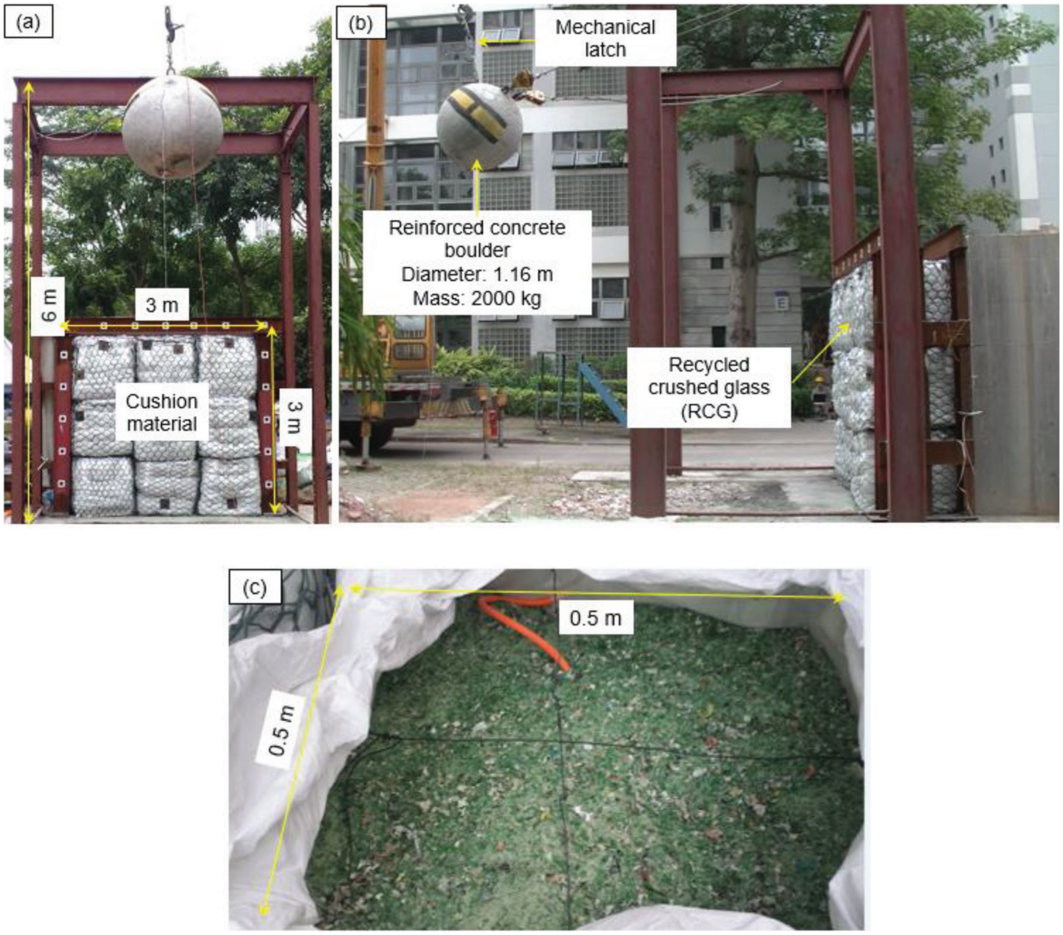

Fig. 2. Front view of rigid barrier and load-cell layout (modified from Ng et al. 2016). (All dimensions in metres.) [Colour online.]

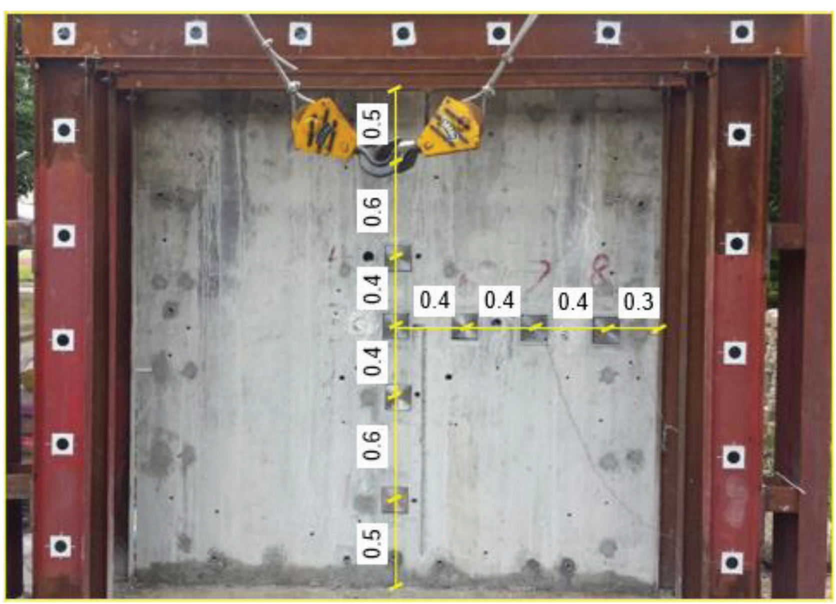

ing was used to select a cutoff frequency of 50 Hz and a low pass filter was adopted to remove the noise from the signal. The deformation of the cushioning material was measured using laser sensors after impact. The data-logging system captured data at a sampling rate of 10 kHz. The impact velocity and penetration depth were estimated using a high-speed camera (Mikrotron, EoSens mini2), which can capture up to 200 frames per second (fps) at a resolution of 1376×1226 pixels. In addition, a video recorder (JVC GX), which can capture images at 30 fps at a resolution of 1920×1080 pixels, was also used to record the impact process.

Table 1. Measured parameters of RCG used in current study.

Parameter	Value
Density (kg/m³)	1500
Debris content	<2% by weight
Particle size (mm)	0.075–20
Young's modulus (MPa)	7.9
Friction angle (°)	38

Properties of RCG

The RCG used in this study was manufactured using a hammer mill. Table 1 lists some of the basic properties of the RCG. Three samples of RCG were tested to measure the average particle-size distribution (PSD). Figure 3 shows three PSD curves of the RCG. The PSD curves show that the RCG satisfies the grading requirements for use as a fill material in Hong Kong (So et al. 2016). The bulk density of RCG is about 1500 kg/m³ and the porosity can be calculated as 44%. Direct shear box tests were conducted to measure the friction angle over a stress range between 50 and 200 kPa. The friction angle was found to be about 38° assuming zero cohesion.

The mechanical response of the RCG under compression was measured using a universal testing machine (AMETEK model No. EZ 50) equipped with a load cell with a maximum range of 25 kN (Fig. 4). A rigid cubical steel box with a nominal dimension of 0.2 m was used to confine the lateral deformation of the RCG specimen during the compression test. The compression rate was selected as 10 mm/min. Figure 5 shows the measured compressive stress–strain curves. Due to the limited loading range of the apparatus, the tests were terminated when the compressive stress reached 625 kPa. The Young's modulus deduced from the initial loading range is about 7.9 MPa. The compressive stress–strain of cellular glass aggregates is also shown in Fig. 5 for comparison. It can be seen that the cellular glass aggregates exhibit large plastic deformation beyond their yield strength due to particle crushing. A higher stress was induced in the cellular glass aggregates (Ng et al. 2018) because the loaded area of cellular glass aggregates was smaller than that of the rigid steel box. The mechanical response of rock fragments contained inside the gabion baskets as reported by Bertrand et al. (2005) is also shown in Fig. 5 for comparison.

Test programme

In this study, a total of 12 impact tests were conducted. Impact energies of 20 and 70 kJ were exerted on a 1 m thick cushion layer of RCG. For each energy level, six successive impact tests were carried out. Table 2 summarizes the test programme. The letter "R" is used to represent RCG. It is worth noting that the cellular glass aggregates tested by Ng et al. (2018) were cubic and are 500 mm long.

Model setup and testing procedures

For the pendulum impact tests, the RCG was placed inside plastic bulk bags that were then placed in steel-wire baskets before they were stacked together to form a 3 m wide, 3 m tall, and 1 m thick cushion layer in front of the reinforced rigid barrier, which was 3 m wide, 3 m tall, and 1.5 m thick. To prevent sagging of the cushion layer, steel wires were weaved through the plastic bags and the layer was attached to the rigid barrier around its perimeter using tie rods (Fig. 1*a*). A high confining stress was generated by the gabion baskets during the impact. The influences of gabion baskets on the mechanical responses are discussed by Lambert et al. (2011).

For each test, the impact energy was controlled by the suspended height of the boulder; that is, 1 m for 20 kJ and 3.5 m for 70 kJ. Once the instrumentation and high-speed cameras were set up, a mechanical latch was used to lift and then release the suspended boulder into the cushion layer.

Fig. 3. Particle-size distribution of RCG. [Colour online.]

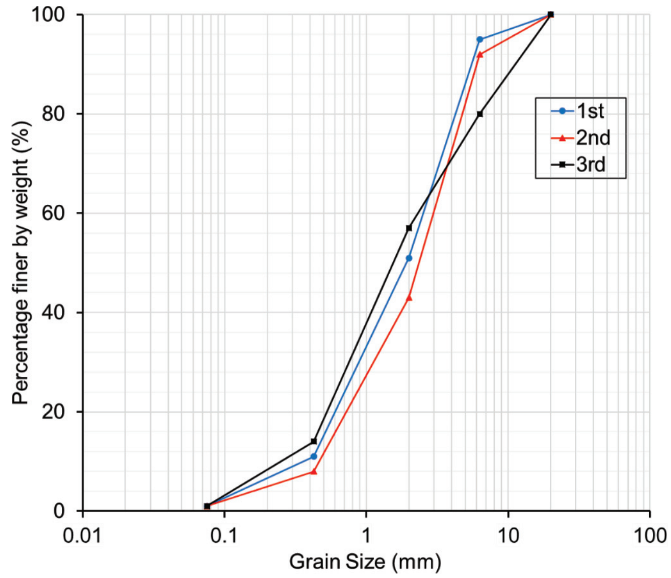

Fig. 4. Compression test setup. [Colour online.]

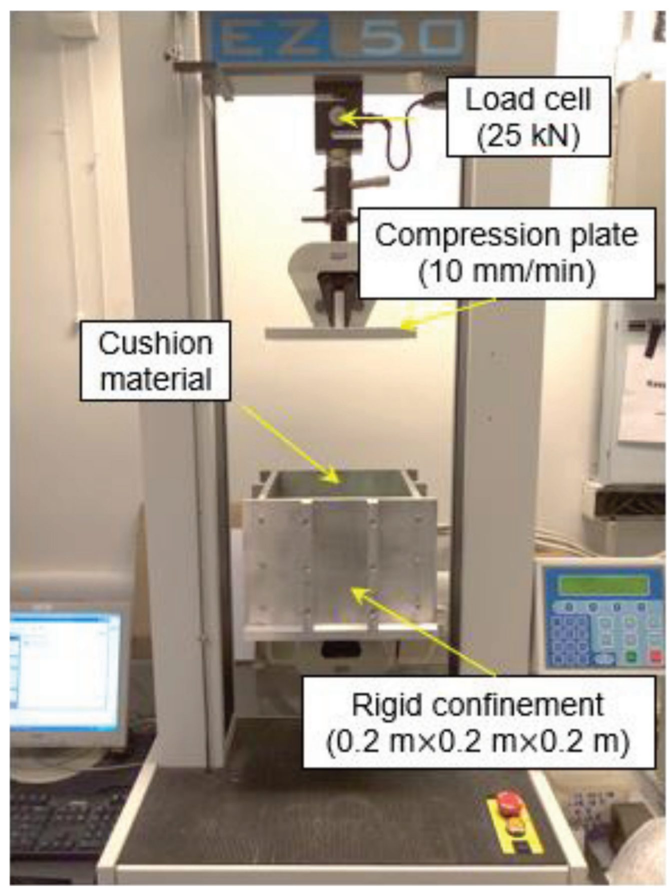

Results and interpretation

Deformation of RCG cushion layer

The deformation of the cushion layer resulting after successive impacts gives an indication of the required thickness of the layer. Figure 6*a* shows a comparison of the measured cumulative deformation profiles for RCG, rock fragments (rock-filled gabions), and cellular glass aggregates, which are denoted as "R", "F", and "C",

Fig. 5. Comparisons of compressive stress–strain curves between rock-filled gabion, cellular glass aggregates, and RCG. [Colour online.]

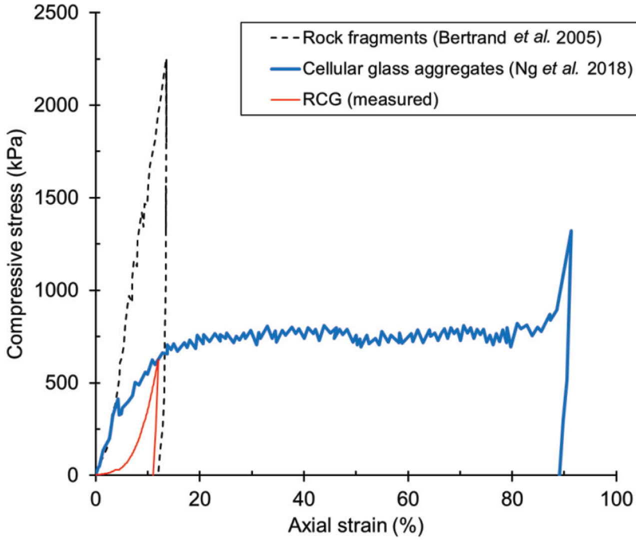

Table 2. Test programme.

Test ID	Impact energy (kJ)	Impact velocity (m/s)	Successive impacts
R-20	20	4.5	6
R-70	70	8.4	6

Fig. 6. Measured penetration depths for rock-filled gabion, cellular glass aggregates, and RCG under successive impacts: (*a*) 20 kJ; (*b*) 70 kJ. [Colour online.]

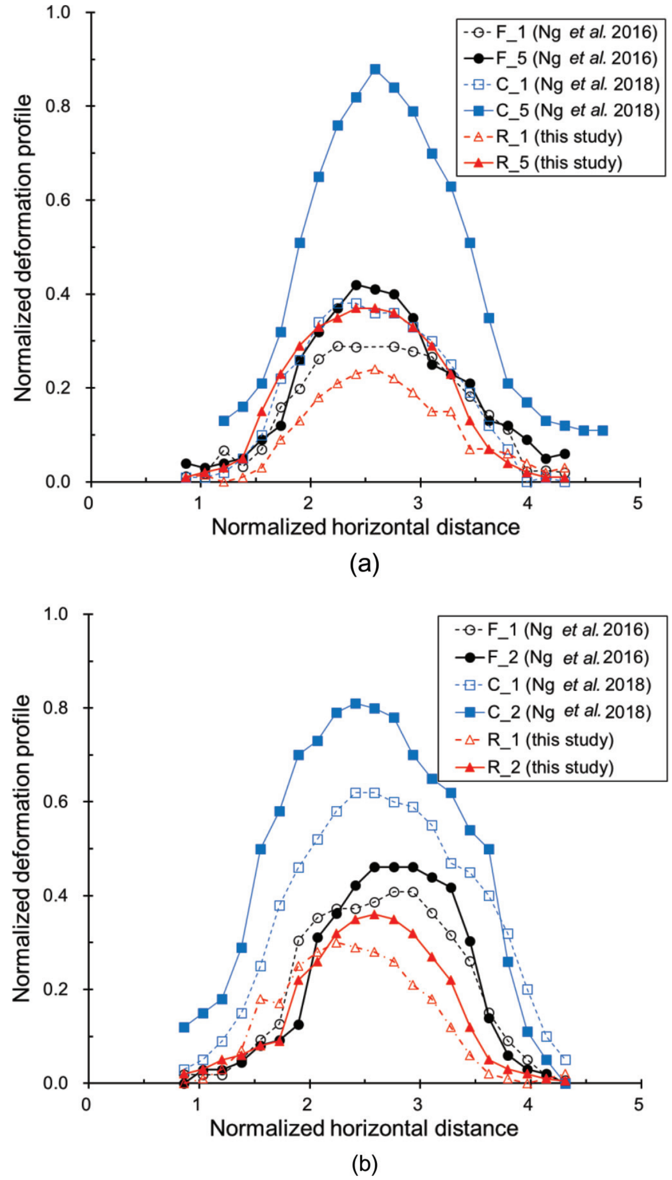

respectively. The measured deformation profiles have been normalized by the thickness of the cushion layer (1 m) to show the mobilized thickness. Furthermore, the width of the cushion layer has also been normalized by the boulder radius of 0.58 m to give a normalized horizontal distance to highlight the impact area relative to the size of the boulder.

Figure 6*a* shows the normalized maximum cumulative deformation (P_{max}) is 0.24 for the RCG during the first impact at an energy level of 20 kJ. In other words, 24% of the cushion thickness was permanently deformed. After the fifth impact, about 37% of the initial RCG thickness was mobilized. The permanent deformation of RCG can be attributed to the irreversible rearrangement and crushing of the glass particles. In contrast, the gabions filled with rock fragments exhibited reduced thicknesses of about 29% and 42% after the first and fifth impacts, respectively. The P_{max} after five successive impacts for the rock fragments is at least 15% larger than that of RCG. One postulation is that the typical particle size of RCG (0.1–20 mm) is much smaller than that of the rock fragments (160–300 mm). Correspondingly, there are a greater number of particle contacts as the particle size decreases. Also, more branching points are generated within the network of force chains (Su et al. 2019). Muthuswamy and Tordesillas (2006) reported that higher loads can be supported by a force chain network that has more branching points. It follows that RCG might have a stronger force–chain network than gabions filled with rock fragments and this may explain the smaller permanent deformation. The result of this comparison also suggests that a thinner cushion layer may be considered if RCG is used compared to rock-filled gabions.

The larger deformation for cellular glass aggregates is due to the fact that these aggregates have a crushing strength of only 0.75 MPa, which is much lower than the crushing strength of RCG. Figure 6*b* shows a comparison of the measured deformation profiles for RCG, rock fragments, and cellular glass aggregates for an impact energy level of 70 kJ. As expected, all the cushioning materials showed increased deformation after the first impact. RCG showed a 25% increase in P_{max} for the first impact when the impact energy is increased from 20 to 70 kJ. The front views of RCG, rock fragments, and cellular glass aggregates for the first impact are shown in Figs. 7*a*, 7*b*, and 7*c*, respectively. Lambert et al. (2011) demonstrated that wire mesh not orientated in the same direction can influence the mechanical response. This observation needs to be taken into account when interpreting the results from this study. A large settlement was observed at the top of the RCG cushion layer, which is caused by the reverse displacement of the central cell. The post-impact face of the RCG cells exhibited a flatter surface than the rock fragment cells. The reverse displacement of the central cell also contributed to the restoration of the cushioning thickness of the cushion layer. An increase in thickness undoubtedly improves the cushioning performance of RCG under successive impacts. This finding suggests that RCG appears to be self-repairing after each boulder impact, if the point of contact is underneath another RCG cell. Smaller settlement was observed for the gabions filled with rock fragments when compared

Fig. 7. Front view of deformed profile after first impact: (*a*) RCG; (*b*) rock-filled gabions; (*c*) cellular glass aggregates. [Colour online.]

with RCG (Fig. 7*b*). These observations imply that reverse displacements also contribute to the cushion thickness of rock fragments. All in all, these results indicate that RCG is more favourable because it offers a more compact solution.

Measured impact force

Figure 8*a* shows the dynamic response of RCG under six successive boulder impacts at an energy level of 20 kJ. The boulder impact force was calculated by multiplying the measured boulder acceleration by the mass of the concrete boulder. The penetration depth was deduced by double integration of the measured boulder acceleration. The red dashed line is used to show the estimated boulder impact forces based on the Hertz equation. For this calculation, a Young's modulus of 7.9 MPa was used (Fig. 5).

The deduced maximum penetration of RCG of 0.28 m is about 15% larger compared to that of the maximum penetration measured at 20 kJ in Fig. 6*a*. The difference is caused by the settlement or self-repairing function observed at the top RCG cell after boulder impact (Fig. 7*a*). The absorbed impact energy, from an input impact energy of 20 kJ, is calculated by successive integration of the measured boulder impact force with respect to the penetration depth. Results indicate that almost the entire boulder impact energy is absorbed by the RCG cushion layer at 20 kJ. This calculated absorbed energy agrees with the observation that there was negligible boulder rebound after impact, as captured using the high-speed camera. An estimated maximum boulder impact force (F_{max}) of 333 kN is deduced using elastic Hertz contact theory and a Young's modulus of 7.9 MPa for the energy level of 20 kJ. It can be seen that F_{max} is overestimated by at least three times when plastic deformation is not considered. Clearly, consideration of plastic deformation induced by the particle rearrangement and crushing is important for interpretation of impact test results.

The densification of RCG is evident during the initial successive impacts, because F_{max} increased by 80% and 40% for the second and third impacts, respectively, when compared with the previous impacts. The effects of densification evidently diminish as only a slight increment of 8% in F_{max} is observed between the fourth and sixth impacts. Large fluctuations in force were observed for each test. Similar observations were also reported by Ng et al. (2016) and Lambert et al. (2014). Furthermore, the calculated energies for successive impacts on RCG are all about 20 kJ, indicating that RCG can provide consistent and stable energy absorption under successive impacts.

Figure 8*b* shows the boulder impact force resulting from successive impacts on RCG at an energy level of 70 kJ. A measured F_{max}

Fig. 8. Dynamic responses of RCG under successive impacts: (*a*) 20 kJ; (*b*) 70 kJ. [Colour online.]

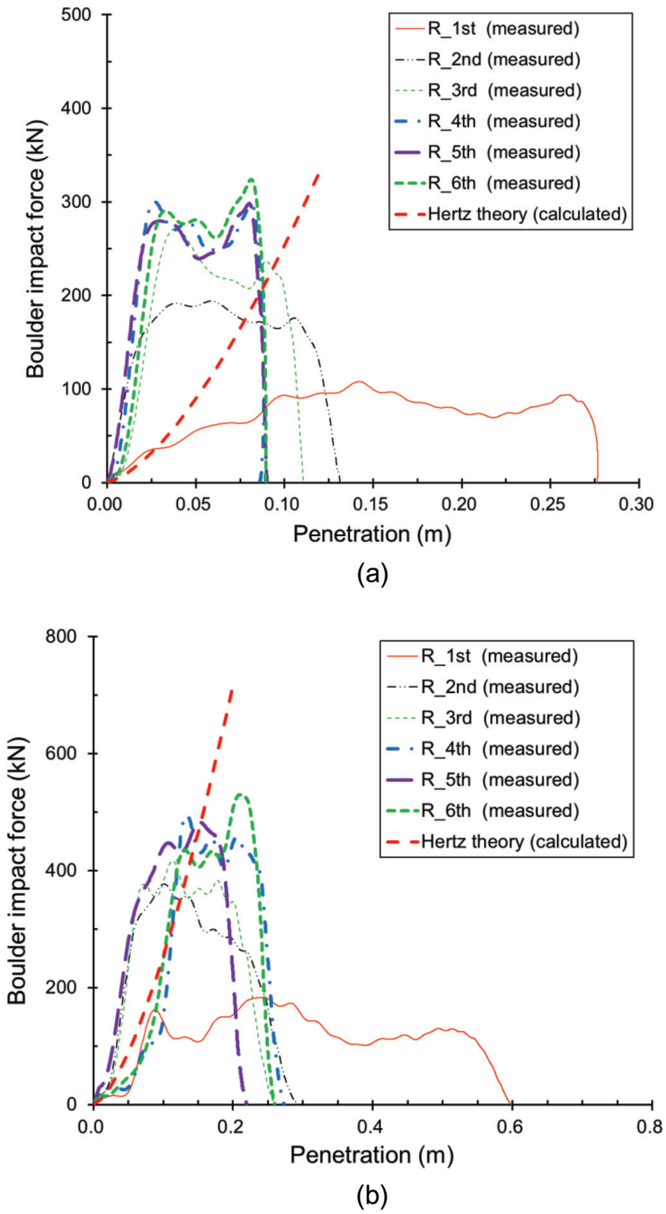

Fig. 9. Performances of cushion layers under successive impacts: (*a*) maximum ball impact force; (*b*) back-calculated load-reduction factor (K_c). [Colour online.]

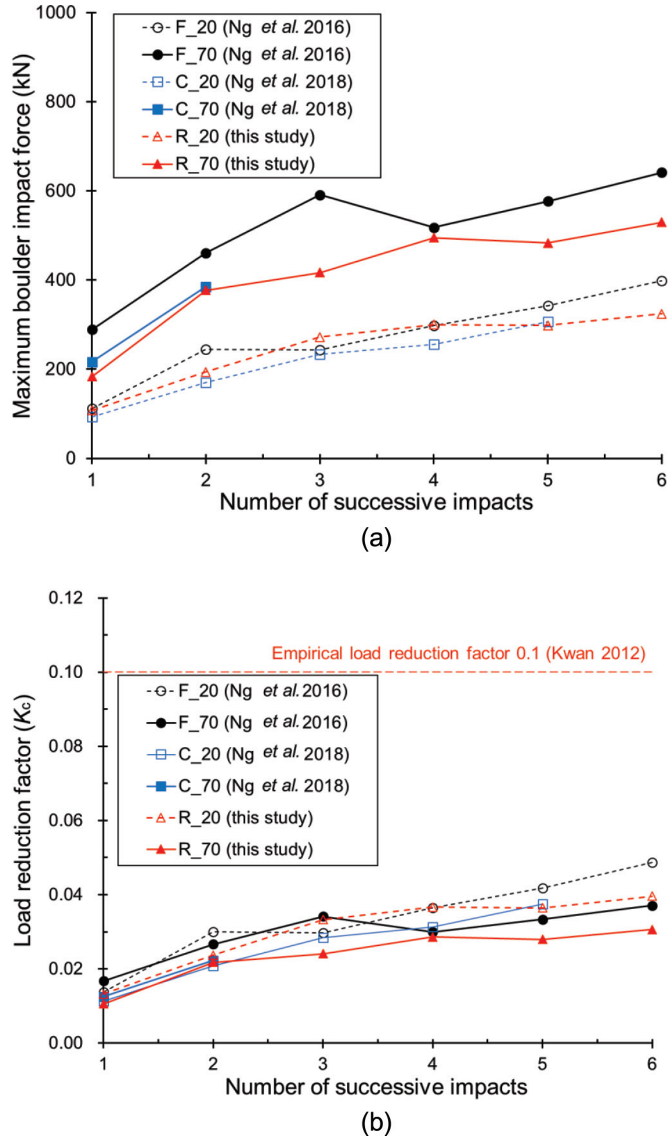

of 183 kN occurs at a penetration of 0.24 m for the first impact. However, a measured P_{max} of 0.3 m (Fig. 6*b*) is only half of the deduced P_{max}, and this was probably caused by the reverse displacement of the RCG cell in the centre of the impact area or the self-repairing effect. This effect is more pronounced at a higher energy level of 70 kJ compared to an energy level of 20 kJ. The large plastic deformation of RCG is mainly caused by particle rearrangement and crushing. These cushioning mechanisms result in a measured F_{max} that is about four times smaller than that estimated using the Hertz contact theory. The F_{max} increased by about 103% and 10% for the second and third impacts, respectively, when compared with that measured at the previous impact. This increase is due to densification of the cushioning material. Similarly for 20 kJ, only a slight increase of 7% is observed from the fourth impact onwards.

Comparisons of F_{max} among RCG, rock fragments, and cellular glass aggregates

Figure 9*a* shows a comparison of the measured F_{max} for RCG, rock fragments (Ng et al. 2016), and cellular glass aggregates (Ng et al. 2018) subjected to successive impacts. The P_{max} on cellular glass aggregates reached 80% of the 1 m thick cushion for the second impact at an energy level of 70 kJ (Fig. 6*b*). To prevent damage to the test setup, only two successive impacts were conducted at 20 kJ. The maximum difference in F_{max} among the three cushioning materials is less than 15% from the third to fifth impacts at an energy level of 20 kJ. This implies that all three cushioning materials provided similar cushioning performance under successive impact loading at 20 kJ. At the higher impact energy level of 70 kJ, the cushioning performance of RCG, based on the measured F_{max}, appears to be the best among the three materials. The measured F_{max} for rock fragments is up to 30% larger than that of RCG from the second impact onwards. This trend was probably caused by the reverse displacement that prevented further reduction in the thickness of the RCG layer (Fig. 7*a*).

Figure 9*b* shows the back-calculated empirical load-reduction factor of K_c under successive impacts for the three cushioning materials. The values of K_c are back-calculated using the measured F_{max} and eq. (2). Normally, K_c is used to estimate the force acting on the rigid barrier, but in this paper its use is extended to com-

Fig. 10. Maximum transmitted load distributions on the rigid barrier at 20 kJ: (*a*) vertical; (*b*) horizontal. [Colour online.]

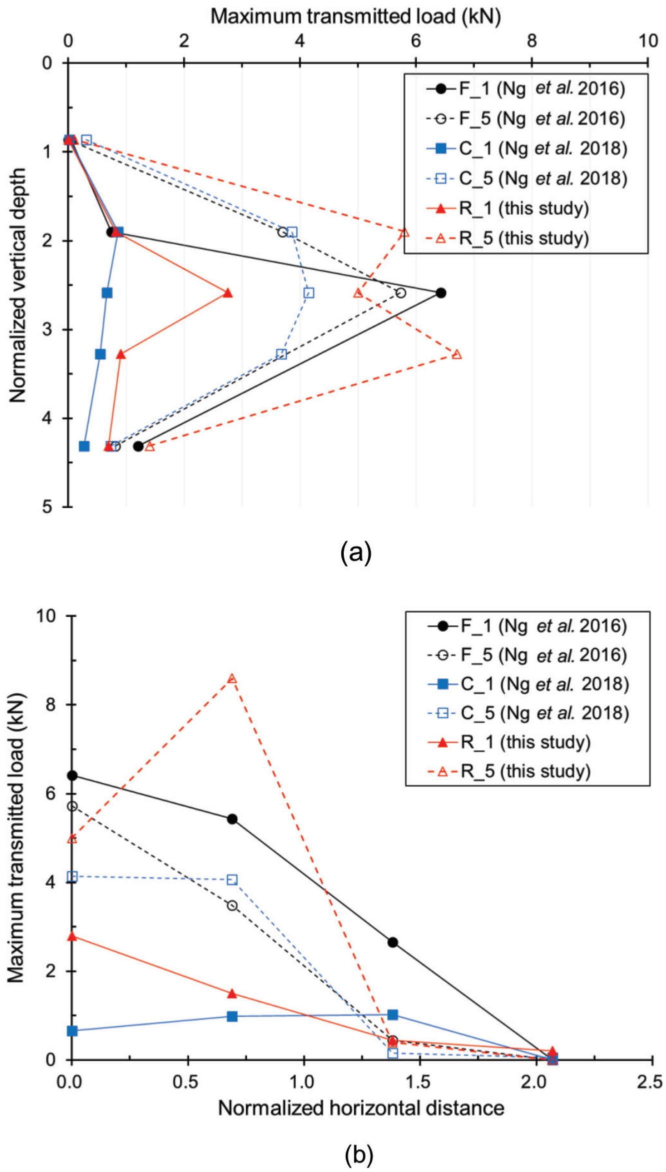

pare the cushion performance among different materials. In a similar manner as F_{max}, the K_c of RCG increases with successive impacts. This increasing trend indicates that the maximum boulder impact force of RCG increases under successive impacts. Furthermore, K_c of RCG at 70 kJ is at least 25% smaller than that of RCG subjected to successive loading at an impact energy of 20 kJ. This implies that a lower maximum boulder impact force is generated on RCG at high impact energy of 70 kJ. This is because higher impact energy induces larger plastic deformation, which improves the overall cushioning performance. It can also be seen that the load-reduction factor of 0.1 proposed by Kwan (2012) for boulders impacting on bare concrete is about three times larger than the back-calculated value of 0.03. This indicates that the maximum boulder impact force could be reduced by about three times when a RCG cushion layer is used.

Transmitted distributed loads on barrier wall

Figures 10*a* and 10*b* show the vertical and horizontal transmitted load distributions, respectively, for RCG, rock fragments, and cellular glass aggregates at 20 kJ. The maximum transmitted load (L_{max}) was measured using load cells embedded in the rigid barrier. The vertical axis in Fig. 10*a* represents the vertical depth on the rigid barrier normalized by the boulder radius. For RCG, a maximum transmitted load of 2.8 kN was measured for the first impact at the centre of rigid barrier. No load is registered by the uppermost load cell. By contrast, L_{max} of 0.7 kN was measured at the normalized height of 4.3. Clearly, the impact load was transmitted downwards more easily. In this regard, a thicker cushion layer can be installed at the bottom of the barrier if a more uniform loading distribution is desired.

For the fifth impact, a L_{max} of 6.7 kN was measured at the normalized depth of 3.3, which is not at the centre of the rigid barrier. A similar counterintuitive location for the maximum transmitted load on the rigid barrier was observed by Ng et al. (2016), and this may be attributed to the self-repairing behaviour of the RCG cushion layer induced by the movements of particles under successive impacts. The L_{max} for the fifth impact is about 2.4 times larger compared with that of the first impact. This coincides with the measured F_{max} under successive impacts. Furthermore, densification of the RCG cushion layer makes contacts between each particle closer, which may result in more loads transmitted on the rigid barrier.

Comparisons between RCG and rock fragments show that the L_{max} of rock fragments is only 14% smaller than RCG for the fifth impact. This suggests that their cushioning performance, based on the transmitted load, is similar for 20 kJ impacts. For cellular glass aggregates, the maximum transmitted load is 40% smaller compared to the RCG for the fifth impact because the cushioning mechanism of cellular glass aggregates is dominated by particle crushing. Overall, among the three cushioning materials cellular glass aggregates show the best cushioning performance in terms of reduction of transmitted loads at the energy level of 20 kJ.

Figure 10*b* shows the horizontal load distributions on the rigid barrier at 20 kJ. The horizontal distance from the centre of the barrier is normalized by the boulder radius. This normalization makes it is easy to compare the load–diffusion capability among the three cushion materials. Likewise, cellular glass aggregates also exhibit the most favorable load-reduction capability in terms of L_{max} for successive impacts.

For the impact energy of 70 kJ, the vertical and horizontal load distributions on the rigid barrier are shown in Figs. 11*a* and 11*b*, respectively. The measured L_{max} of RCG is 3.6 kN at the normalized distance of 2.6 for the first impact. For the sixth impact, L_{max} is up to 3.9 times larger than that of the first impact at the centre of RCG. RCG performs better than rock fragments based on the boulder impact force and transmitted load on the rigid barrier. This is because the particle size of RCG is much smaller compared to the particle size of rock fragments. Zhang et al. (2016, 2017) suggested that transmitted loads decrease with the particle size because the force chains are more stable. Furthermore, smaller particles tend to favour load diffusion (Su et al. 2019). Together, these effects contribute to the reduction of the transmitted load. Furthermore, the reverse displacement of RCG after each impact also improves the cushioning performance under successive impacts.

Figure 11*b* shows the measured horizontal load distributions on the rigid barrier at 70 kJ. For RCG, L_{max} of 0.4 and 0.2 kN were measured at the normalized distances of 1.4 and 2.1, respectively. Comparatively, no load was measured at the same horizontal distance for the cellular glass aggregates. This can be attributed to the distinct cushioning mechanisms between these two materials. For cellular glass aggregates, the cushioning mechanism is mainly dominated by crushing, which leads to higher transmitted loads concentrated at the centre of rigid barrier. By contrast, both particle rearrangements and crushing contribute to the cushioning performance of RCG. Both of these features enable more uniform transmitted loads on the rigid barrier. Due to the limited number of load cells installed on the rigid barrier, the exact load–

Fig. 11. Maximum transmitted load distributions on the rigid barrier at 70 kJ: (*a*) vertical; (*b*) horizontal. [Colour online.]

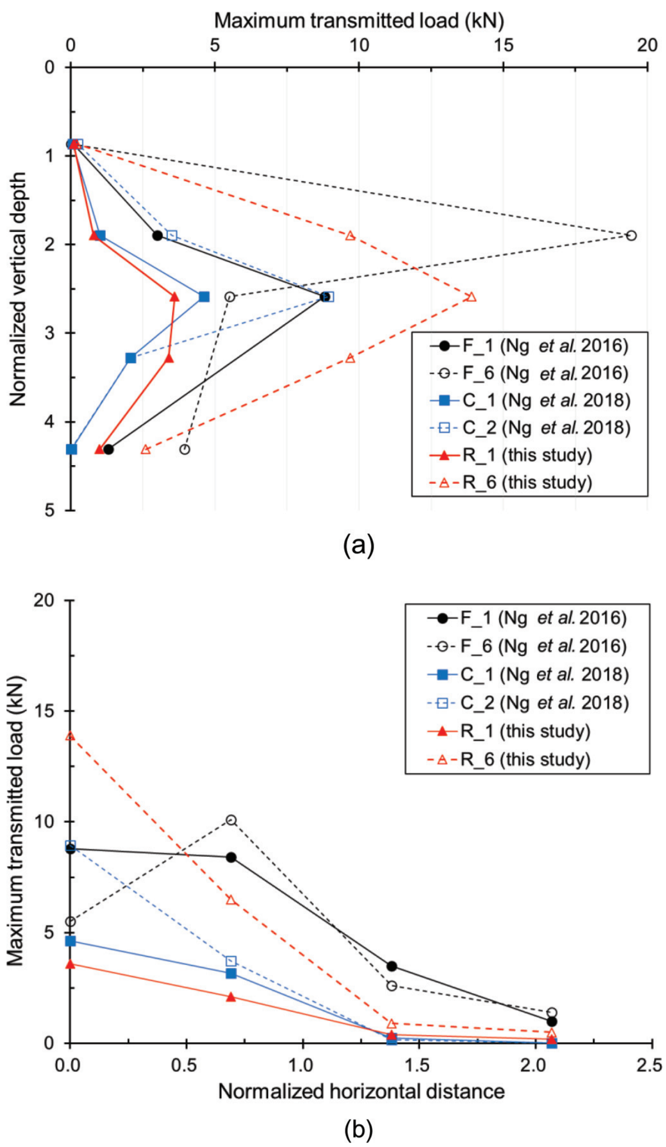

diffusion angle cannot be obtained. However, an estimated load–diffusion angle, α, of 32° can be derived for RCG if the maximum load diffusion is assumed to reach the maximum normalized horizontal distance of 2.1 (Fig. 12). This diffusion angle of RCG is almost three times higher than that derived for cellular glass aggregates (Ng et al. 2018). Comparisons between the results for rock fragments and RCG also show that the slopes of load distribution profiles for rock fragments are much steeper than those for RCG. This suggests that more load is distributed by RCG compared to rock fragments. For the sixth impact, the L_{max} of rock fragments is smaller than the first impact. As discussed above, this may be attributed to the uneven contacts between the rock fragments and the rigid barrier. In terms of the reductions of L_{max} and the load–diffusion angle, it appears that RCG gives the best cushioning performance for the impact energy of 70 kJ.

Conclusions

A series of large-scale pendulum impact tests have been carried out to study the cushioning performance of RCG under successive impacts at energy levels of up to 70 kJ. A summary of the key findings is given as follows:

Fig. 12. Schematic diagram of load diffusion.

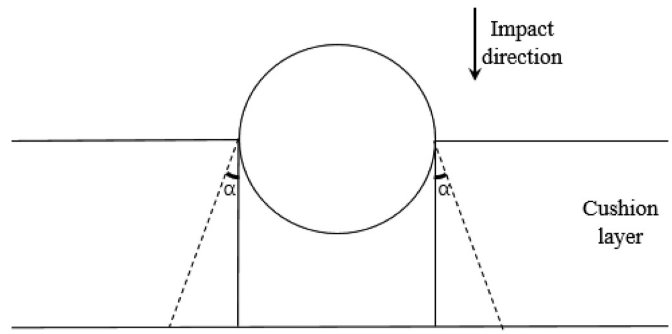

1. The test results show that when RCG is used, the maximum boulder impact forces (F_{max}) for the first impact are 128% and 41% less than that for rock fragments (rock-filled gabions) and cellular glass aggregates, respectively. From the second to sixth impacts, the F_{max} of RCG is up to 30% smaller than that of rock-filled gabions. These results suggest that RCG is more effective in reducing boulder impacts at 70 kJ compared to rock fragments and cellular glass aggregates. The reverse displacement of RCG is believed to play a role in its good cushioning performance compared to the other two cushioning materials under successive impacts.
2. For a RCG cushion layer subjected to successive boulder impacts at 70 kJ, the back-calculated load-reduction factor for the sixth impact is 0.03. This value is considerably smaller than the current design value of 0.1 suggested for boulder impacts on bare concrete. This implies that the design boulder impact load could be reduced by about three times if RCG is used to protect a debris-resisting rigid barrier.
3. Among the three cushioning materials evaluated in this study, RCG exhibits the best overall cushioning performance in terms of the reduction of the maximum transmitted load on the barrier wall (L_{max}) and the load–diffusion capability at an energy level of 70 kJ. Results reveal that the measured L_{max} of RCG is 144% and 12% smaller than that of rock fragments and cellular glass aggregates for the first impact, respectively. The load–diffusion angle of RCG is almost three times larger than that of cellular glass aggregates.
4. Based on the results presented in this study, it may be concluded that RCG is a new and promising material to adopt for shielding barriers in mountainous regions around the world. However, it should be noted that this study only focuses on the technical aspect of RCG for impact energies up to 70 kJ. Higher energy levels should also be considered if RCG is used in practice. In addition, the health and safety aspects must also be carefully considered if RCG is used.

Acknowledgements

This paper is published with the permission of the Head of the Geotechnical Engineering Office and the Director of Civil Engineering and Development, the Government of the Hong Kong Special Administrative Region (SAR), China. The authors are grateful for financial support from the theme-based research grant T22-603/15N and the general research fund 16209717 provided by the Research Grants Council of the Government of the Hong Kong SAR, China. The authors are also grateful for the financial sponsorship from the National Natural Science Foundation of China (51709052). The support of the HKUST Jockey Club Institute for Advanced Study and the financial support of the Hong Kong Jockey Club Disaster Preparedness and Response Institute (HKJCDPRI18EG01) are gratefully acknowledged.

References

ASTRA. 2008. Effects of rockfall on protection galleries. Federal Roads Office, Switzerland.

Bertrand, D., Nicot, F., Gotteland, P., and Lambert, S. 2005. Modelling a geocomposite cell using discrete analysis. Computers and Geotechnics, **32**(8): 564–577.

Breugnot, A., Lambert, S., Villard, P., and Gotteland, P. 2015. A discrete/continuous coupled approach for modeling impacts on cellular geostructures. Rock Mechanics and Rock Engineering, **49**(5): 1831–1848. doi:10.1007/s00603-015-0886-8.

GEO. 1993. Guide to retaining wall design (Geoguide 1). Geotechnical Engineering Office (GEO), the Government of the Hong Kong Special Administrative Region.

Heymann, A., Lambert, S., Haza-Rozier, E., Vinceslas, G., and Gotteland, P. 2010. An experimental comparison of half-scale rockfall protection sandwich structures. *In* Proceedings, Structures under Shock and Impact XI-SUSI XI, Tallinn, Estonia, WIT Press, Southampton, UK.

Hungr, O., Morgan, G.C., and Kellerhals, R. 1984. Quantitative analysis of debris torrent hazards for design of remedial measures. Canadian Geotechnical Journal, **21**(4): 663–677. doi:10.1139/t84-073.

Iverson, R.M. 1997. The physics of debris flows. Reviews of Geophysics, **35**(3): 245–296. doi:10.1029/97RG00426.

Johnson, K.L. 1985. Contact mechanics. Cambridge University Press, London, UK.

Kwan, J.S.H. 2012. Supplementary technical guidance on design of rigid debris-resisting barriers. GEO Report No. 270, Geotechnical Engineering Office, the Government of the Hong Kong Special Administrative Region.

Kwan, J.S.H., Sze, E.H.Y., and Lam, C. 2019. Finite element analysis for rockfall and debris flow mitigation works. Canadian Geotechnical Journal. [Published online ahead of print 14 July 2018.] doi:10.1139/cgj-2017-0628.

Lam, C.S., Poon, C.S., and Chan, D. 2007. Enhancing the performance of pre-cast concrete blocks by incorporating waste glass – ASR consideration. Cement and Concrete Composites, **29**(8): 616–625. doi:10.1016/j.cemconcomp.2007.03.008.

Lam, C., Kwan, J.S.H., Su, Y., Choi, C.E., and Ng, C.W.W. 2018. Performance of ethylene-vinyl acetate foam as cushioning material for rigid debris-resisting barriers. Landslides, **15**(9): 1779–1786. doi:10.1007/s10346-018-0987-z.

Lambert, S., Gotteland, P., and Nicot, F. 2009. Experimental study of the impact response of geocells as components of rockfall protection embankments. Natural Hazards and Earth System Sciences, **9**(2): 459–467. doi:10.5194/nhess-9-459-2009.

Lambert, S., Nicot, F., and Gotteland, P. 2011. Uniaxial compressive behavior of scrapped-tire and sand-filled wire netted geocell with a geotextile envelope. Geotextiles and Geomembranes, **29**(5): 483–490. doi:10.1016/j.geotexmem.2011.04.001.

Lambert, S., Heymann, A., Gotteland, P., and Nicot, F. 2014. Real-scale investigation of the kinematic response of a rockfall protection embankment. Natural Hazards and Earth System Sciences, **14**(5): 1269–1281. doi:10.5194/nhess-14-1269-2014.

Lo, D.O.K. 2000. Review of natural terrain landslide debris-resisting barrier design. GEO Report No. 104, Geotechnical Engineering Office, Hong Kong Special Administrative Region.

Méar, F., Yot, P., Cambon, M., and Ribes, M. 2006. The characterization of waste cathode-ray tube glass. Waste Management, **26**(12): 1468–1476. doi:10.1016/j.wasman.2005.11.017. PMID:16427267.

Muthuswamy, M., and Tordesillas, A. 2006. How do interparticle contact friction, packing density and degree of polydispersity affect force propagation in particulate assemblies? Journal of Statistical Mechanics: Theory and Experiment, **2006**(9): P09003. doi:10.1088/1742-5468/2006/09/P09003.

Ng, C.W.W., Choi, C.E., Su, A.Y., Kwan, J.S.H., and Lam, C. 2016. Large-scale successive boulder impacts on a rigid barrier shielded by gabions. Canadian Geotechnical Journal, **53**(10): 1688–1699. doi:10.1139/cgj-2016-0073.

Ng, C.W.W., Su, Y., Choi, C.E., Song, D., Lam, C., Kwan, J.S.H., Chen, R., and Liu, H. 2018. Comparison of cushion mechanisms between cellular glass and gabions subjected to successive boulder impacts. Journal of Geotechnical and Geoenvironmental Engineering, **144**(9). doi:10.1061/(ASCE)GT.1943-5606.0001922.

Schellenberg, K., Volkwein, A., Roth, A., and Vogel, T. 2006. Rockfall-falling weight tests on galleries with special cushion layers. *In* Proceedings, 3rd International Conference on Protection of Structures against Hazards, pp. 1–8.

Schellenberg, K., Volkwein, A., Roth, A., and Vogel, T. 2007. Large-scale impact tests on rock fall galleries. *In* Proceedings, 7th International Conference on Shock and Impact Loads on Structures, Beijing, China, pp. 497–504.

Shi, C., Wu, Y., Riefler, C., and Wang, H. 2005. Characteristics and pozzolanic reactivity of glass powders. Cement and Concrete Research, **35**(5): 987–993. doi:10.1016/j.cemconres.2004.05.015.

So, S.T.C., Hui, T.H.H., and Lee, R.M.K. 2016. Technical feasibility of using glass cullet as an engineering fill in reclamation and earthworks. GEO Report No. 324, Geotechnical Engineering Office, the Government of the Hong Kong Special Administrative Region.

Srivastava, V. 2014. Glass wastes as coarse aggregate in concrete. Journal of Environmental Nanotechnology, **3**(1): 67–71. doi:10.13074/jent.2013.12.132059.

Su, Y., Cui, Y., Ng, C.W.W., Choi, C.E., and Kwan, J.S.H. 2019. Effects of particle size and cushioning thickness on the performance of rock-filled gabions used in protection against boulder impact. Canadian Geotechnical Journal, **56**(2): 198–207. doi:10.1139/cgj-2017-0370.

Takahashi, T. 2014. Debris flow: mechanics, prediction and countermeasures. CRC Press.

Zhang, L., Nguyen, N.G.H., Lambert, S., Nicot, F., Prunier, F., and Djeran-Maigre, I. 2016. The role of force chains in granular materials: from statics to dynamics. European Journal of Environmental and Civil Engineering, **21**(7–8): 874–895.

Zhang, L., Lambert, S., and Nicot, F. 2017. Discrete dynamic modelling of the mechanical behaviour of a granular soil. International Journal of Impact Engineering, **103**: 76–89. doi:10.1016/j.ijimpeng.2017.01.009.

Zhang, S., Hungr, O., and Slaymaker, O. 1996. The calculation of impact force of boulders in debris flow. *In* Debris flow observation and research. *Edited by* R. Du. Science Press, pp. 67–72. [In Chinese.]